



Electroanalytical application of phenol-functionalized reduced graphene oxide produced using gallic acid in a single step

Mónica Moreno^{*}, Alberto Sánchez Arribas^{*}, Silvia Royano, Yaiza Izquierdo, Manuel Chicharro

Dpto. Química Analítica y Análisis Instrumental, Universidad Autónoma de Madrid, C/Francisco Tomás y Valiente 7, Madrid, Spain

ARTICLE INFO

Keywords:

Graphene
Adsorptive Stripping Voltammetry
Gallic acid
Functionalization
Dopamine
Uric acid

ABSTRACT

This study introduces a simple one-step approach for synthesizing phenol-functionalized reduced graphene oxide for electroanalytical purposes, just using gallic acid (GA) and graphene oxide (GO). GA serves as both a reductant for GO and a stabilizing, functionalizing agent, introducing phenolic groups to the nanomaterial. This functionalization imparts remarkable attributes to the nanomaterial, allowing complete dispersion in aqueous solutions and tuning of its electrochemical performance, making it very convenient for electrode modification. The resulting nanomaterials (GA-rGO) underwent characterization through UV-visible, Fourier-transform infrared (FTIR), and Raman spectroscopies, as well as scanning electron microscopy (SEM). Glassy carbon electrodes modified with aqueous dispersions of these nanomaterials (GA-rGO/GCE) were employed in voltammetric experiments to evaluate the optimal dispersion composition for electroanalytical application.

These GA-rGO/GCE displayed high electrocatalytic activity for the electrochemical oxidation of relevant clinical and environmental analytes. The unique functionalization of GA-rGO facilitated the selective accumulation of dopamine (DA) and uric acid (UA) on the electrode surface, even in the presence of significant amounts of ascorbic acid (AA) in mixtures. Under the specified conditions, voltammetric currents display linear increments over the concentration ranges of 3.0×10^{-7} M to 2.0×10^{-5} M for DA and 7.0×10^{-6} M to 1.0×10^{-4} M for UA. The sensor demonstrated a low detection limit of 0.090 and 2.1 μ M for DA and UA, respectively. The reliability of the electroanalytical performance of the proposed sensor in real samples was demonstrated by the quantification of DA in medications, as well as DA and UA in human urine samples, yielding recovery values between 82 % and 105 %, with relative standard deviation below 11 %.

Introduction

Graphene is a well-known 2D layered material, which exhibits extraordinary electrical conductivity, large surface-to-volume ratio, unique optical/vibrational modes, exceptional mechanical strength, and excellent biocompatibility. These properties have drawn increasing interest for use in biochemical sensing applications [1,2]. The inert electrochemistry, wide potential window, and electrocatalytic properties, combined with the high surface area to volume ratio of this 2D material, makes it an attractive component of the sensing interface in the development of electrochemical sensors [3,4].

Production of individual graphene layers has been reported using several physical and chemical methods, including chemical and mechanical graphite exfoliation [5], chemical vapor deposition (CVD), [6,7], “unzipping” of carbon nanotubes, and graphitization of silicon carbide (SiC) [8]. All these methods can produce graphene layers similar

to the pristine graphene structure. However, the lack of scalability, complex control processes, ultrahigh temperatures, or vacuum requirements, and consequently, the high cost of these methods had limited the adoption of graphene in electrochemical sensors and biosensors. [2,4].

However, efficient, and cost-effective production of bulky graphene sheets is achieved from graphite through its chemical oxidation to graphite oxide, exfoliation of graphene oxide (GO) and subsequent chemical reduction of the exfoliated material. The presence of epoxy, carboxylic and hydroxyl functional groups on the basal plane of GO makes it hydrophilic, allowing the dispersion of single-layered or few-layered GO in water [9]. The disrupted sp^2 bonding networks of GO sheets make them electronically nonconductive. However, the subsequent reduction of GO to conductive graphene can be done by removing the oxygen functional groups. This process can be carried out by employing chemical, thermal, or electrochemical approaches.

^{*} Corresponding author.

E-mail addresses: monica.moreno@uam.es (M. Moreno), alberto.sanchez@uam.es (A. Sánchez Arribas).

<https://doi.org/10.1016/j.flatc.2023.100605>

Received 11 October 2023; Received in revised form 15 December 2023; Accepted 30 December 2023

Available online 9 January 2024

2452-2627/© 2023 The Author(s). Published by Elsevier B.V. This is an open access article under the CC BY-NC-ND license (<http://creativecommons.org/licenses/by-nc-nd/4.0/>).

Depending on the utilized reduction method, the produced reduced graphene oxide (rGO) may have different characteristics in terms of defects (vacancies and holes) and the carbon to oxygen ratio (C/O), which plays a critical role in many properties of the final product [4,9].

Chemical reduction is cheap and easy, as it can be performed using simple equipment at room temperature or under rather average heating condition just by adding liquid reducing reagents to a GO aqueous dispersion [10,11]. The major drawback of the traditional routes for the chemical reduction of GO is the use of toxic and hazardous chemicals, both to living organisms and the environment. Chemical reagents can be eliminated when employing the electrochemical method. In this case, the reduction process relies on the GO-electrode electron exchange and it can be performed inside an electrochemical cell in the presence of an aqueous buffer solution. On the other hand, the mass production of rGO using electrochemical methods is challenging, and the obtained rGO retains the defects and vacancies from the precursor GO, as well as some oxygen functionalities that can't be fully removed by this mean.

Finally, thermal reduction of GO can be produced by rapid annealing at high temperatures under inert gas, inducing the removal of oxygen functionalities in multistep processes. Heating rate, temperature, and time strongly affect the properties of the product and, for example, temperatures as high as 1100 °C are recommended to obtain high-quality rGO with good conductive properties [12]. Therefore, these methods are somewhat expensive and complicated. Microwave- and photo-assisted procedures [13,14] are further used to assist the thermal reduction method as they present the advantage of rapid and uniform heating of substances using microwave ovens and photo-irradiation with various lasers [10,11].

The incorporation of graphene into electroanalytical platforms is mostly achieved as a modifying layer of nanomaterial on top of a supporting electrode such as a glassy carbon (GCE) or a screen-printed carbon electrode (SPCE). However, fewer examples of free-standing graphene paper electrodes and composite electrodes have been reported [15]. Modification of electrodes with a graphene thin layer is typically obtained by drop-casting from a suitable dispersion of nanomaterial, usually as rGO produced by chemical or thermal reduction. Additionally, the production of rGO films by direct electrochemical reduction from either an aqueous GO dispersion or a pre-casted GO deposit has emerged as an advantageous and convenient approach for these purposes. However, it is widely reported that the electrochemical properties and performance of these graphene-based devices strongly depend on nanomaterial's flake/lateral size, the number of stacked layers, the manufacturing process and the resulting edge-plane like-sites, defects, and contaminant content, and by its geometry/structure [16–18]. Therefore, a rich yet variable electrochemistry has been observed in these graphene nanomaterials, offering wide electroanalytical possibilities but leading to inconsistent and contradictory conclusions regarding to their electrocatalytic properties.

Functionalization of graphene under appropriate conditions is an alternative for better controlling of the properties of produced materials. Thereby, nanomaterial dispersibility can be selectively tuned and enhanced, self-stacking of graphene layers and agglomeration issues can be prevented, and even the sp^2 -hybridized carbon lattice can be restored and protected. Moreover, the presence of oxygen groups can be tailored to promote those with favored chemical or electrochemical characteristics, and new functional groups can be introduced, conferring new properties or serving as anchoring sites for molecules and other nanoparticles [17,19,20]. Modification of graphene surface is mainly carried out following covalent and non-covalent functionalization strategies, as well as elemental doping. Therefore, countless methods have been developed so far. One interesting alternative to produce rGO with controlled properties is using appropriate reagents for GO reduction that simultaneously adsorb to the surface of the produced nanomaterial, acting as stabilizing agents and preventing its agglomeration. This strategy has some attractive advantages, namely: 1) enhanced dispersibility and stability of the produced nanomaterial; 2)

environmental-friendly production and biocompatibility, as green reducing agents are employed; 3) introduction of new functionalities; and 4) tailored properties (electrical, optical, or affinity, among others) [21,22]. Therefore, functionalized rGO materials have been produced using bioactive compounds such as melatonin [23], dopamine [24], cysteine [25], or glutathione [26], polysaccharides such as starch [27,28], polyphenolic compounds like 3-hydroxyflavone derivatives [22], tannic acid [29,30], gallic acid [31], resveratrol [32,33], or curcumin [34,35], and different polyphenol-rich plant extracts [36] for different purposes.

In this work we propose the production of a functionalized rGO material to be used as electrode surface modifier for electroanalytical purposes. Gallic acid (GA) was selected as an efficient, yet sustainable, reducing reagent that also served as a stabilizing and functionalization element, introducing phenolic groups to the nanomaterial. The presence of these functional groups decisively improves the electrochemical performance of electrodes modified with such functionalized rGO towards certain molecules, as demonstrated for relevant analytes such as hydrazine (HZ), uric acid (UA), and dopamine (DA). Other rGO materials involving GA in their production have been recently employed for energy storage devices [37] and transparent conductive film heaters [38]. However, the electroanalytical possibilities towards these analytes have not yet been explored.

Materials and methods

Reagents, solutions, and samples

Gallic acid, uric acid sodium salt, 3-hydroxytyramine (dopamine) hydrochloride, and hydrazine sulphate were supplied by Sigma-Aldrich (Madrid, Spain) whereas L-(+)-ascorbic acid, potassium ferrocyanide, and potassium ferricyanide were from Panreac (Barcelona, Spain). All the other chemicals were analytical-reagent grade and were used without further purification. Ultrapure water ($\rho > 18 \text{ M}\Omega \text{ cm}$) was produced by an Elga Purelab Option Q system (ELGA LabWater; UK) and was used to prepare all aqueous solutions. Phosphate buffer solutions were obtained using appropriate amounts of phosphoric acid, from Scharlab (Sentmenat, Spain), and the desired pH was adjusted by adding 1.0 M NaOH before being made up to their final volume with water.

An enzymatic colorimetric kit for the determination of uric acid (Cat. No. UA 230) was acquired from Randox Laboratories Ltd (Crumlin, UK). The method is based on the conversion of uric acid to allantoin and hydrogen peroxide by uricase enzyme, and subsequent peroxidase-catalyzed formation of a red-violet quinoneimine compound from hydrogen peroxide and dye compounds. This kit is suitable for uric acid evaluation in serum, plasma, and urine samples.

Graphene oxide powder from Sigma (Madrid, Spain; Cat. No. 763713), with purity higher than 95 %, was employed in the synthesis of reduced graphene oxide (rGO).

Dopamine hydrochloride injection ampules (200 mg /5 mL) were from Grifols Laboratory (Barcelona, Spain). Fresh urine samples from a volunteer donor were collected and centrifuged to precipitate proteins. Then, fractions of 10.0 mL of filtered urine were stored under refrigeration. Dopamine hydrochloride injection samples and urine samples were suitably diluted either with supporting electrolyte or mobile phase before voltammetric or chromatographic analysis, respectively. Urine samples were spiked with suitable volumes of dopamine standard solution to obtain the desired concentrations.

Apparatus

Electrochemical measurements were carried out using either a BAS 100B (BAS; West Lafayette, USA) electrochemical analyzer controlled by BAS W 2.3 software (BAS; West Lafayette, USA) or a μ AUTOLAB type III electrochemical analyzer controlled by GEPES 4.9.007 software (Eco Chemie; Utrecht, Netherlands).

Spectrophotometric measurements were conducted using a double-beam spectrophotometer Jasco V-630 (Japan) controlled by SPECTRA MANAGER 2.08.04 software.

The pH was monitored with a glass electrode connected to a 913 pH Meter instrument from Metrohm.

Fourier-transform infrared (FTIR) spectra were acquired using a Bruker IFS66v FTIR spectrometer (Bruker; Ettlingen, Germany) in the transmittance mode.

Raman spectroscopy experiments were carried out using an Enwave Optonics Pro-Raman L equipment with a green laser ($\lambda = 532$ nm), coupled to an Olympus BX51 M microscope.

High-performance liquid chromatography (HPLC) separations were carried out using an X-LC chromatograph (JASCO, Japan), which consisted of an XL-C3080DG degasser, an XL-C 3185PU isocratic pump, an X-LC 3167 column oven, and an X-LC3110 diode array detector. The separation column was a 100 mm x 3.0 mm Kinetex 2.6 μ m C18 column equipped with a C18 filter security guard system (Phenomenex; Torrance, USA). Samples were introduced by a Rheodyne 7725i manual valve with a 5.0 μ L sample loop. Chromatograms were acquired with ChromNav software (JASCO, Japan).

Freeze-drying of reduced graphene oxide samples was achieved with a Telstar Lyobeta-15 lyophilizer (Telstar, Spain).

Ultrasonic treatments were carried out either using an ultrasonic probe (Sonics Vibra Cell, model VCX130; Sonics & Materials, Inc; Newtown, CT, USA) or an ultrasonic bath (Ultrasons, model 3000512; JP Selecta, Barcelona, Spain).

Field emission scanning electron microscopy (FE-SEM) images were obtained using an Electron Beam Lithography eLINE-PLUS (Raith GmbH; Dortmund, Germany) system equipped with FE-SEM image acquisition and an energy dispersive spectroscopy (EDS) analyzer XFlash 6–30 (Bruker).

Modification of electrodes

Preparation of phenol functionalized reduced graphene oxide (GA-rGO) and its dispersions

The GA-rGO was prepared as follows: firstly, 2.0 mg of commercial GO were dispersed in 8.0 mL of water by applying an ultrasonic treatment at 2000 J. Then, 20 mg of GA and 30 μ L of concentrated NH_3 (25 % w/w) were added. After sonication for 60 min in an ultrasonic bath, the mixture was maintained at 80 °C for 6.0 h, typically. The dispersion was centrifuged at 9000 rpm for 60 min, resulting in a brown precipitate and a greenish-yellow supernatant. Subsequently, the supernatant containing excess GA was removed, and the precipitate was collected in 1.0 mL of pure water through ultrasonic treatment in a bath for 10 min. These dispersions were further diluted with water according to selected conditions for either electrode modification or spectrophotometric experiments.

Preparation of hydrazine-reduced GO dispersion (HZ-rGO)

The procedure was the same as GA-rGO, except GA was substituted by 5.6 mg of hydrazine sulfate, in order to keep the hydrazine to GO weight ratio close to 7:10 [39].

Electrode treatment and modification process

Glassy carbon electrodes (GCE; model CHI104, 3-mm diameter) were supplied by CH Instruments (Austin, TX, USA). They were polished with 0.3- and 0.05- μ m alumina slurries (Buehler; Spain) on polishing cloths (Buehler; Spain) and subjected to ultrasonic cleaning in water for 1 min before use. Modification of the GCE with graphene films was achieved by dropping 5.0 μ L of any graphene dispersion onto clean GCE surface and allowing it to dry for at least 2 h. Glassy carbon rods of 3-mm diameter (Godfellow; Huntingdon, UK) were modified in the same way for microscopy experiments.

Electrochemically-reduced graphene oxide modified electrodes (ERGO/GCE) were prepared using a GCE modified with 5.0 μ L of GO

dispersion in water (0.5 mg mL⁻¹), which was subsequently placed in a three-electrode electrochemical cell containing 0.050 M phosphate buffer (pH 7.0) and then subjected to voltammetric treatment with 10 cycles from 0.00 V to -1.20 V at a scan rate of 0.050 V s⁻¹. This treatment allowed the electrochemical reduction of casted GO, and these ERGO/GCE were then ready for electrochemical measurements.

Measurement procedures

Electrochemical measurements

Cyclic voltammetry experiments were conducted at room temperature under quiescent conditions using a standard three-electrode cell (10 mL) system. Either bare or modified GCE were used as the working electrode, while an Ag/AgCl/3M NaCl (model RE-1B ALS Co. Ltd.; Tokyo, Japan) and a platinum wire (1-mm diameter) were the reference and auxiliary electrodes, respectively. The potentials given in these experiments were referenced to this electrode system. Before any voltammetric measurement, an electrochemical pretreatment (10 scans between -0.20 and + 1.00 V in fresh supporting electrolyte) was carried out to obtain a stable background signal. Voltammograms were recorded at a scan rate of 0.050 V s⁻¹, typically from -0.20 to + 0.80 V, starting in the anodic direction.

The supporting electrolyte was 0.050 M phosphate buffer (pH 7.0), and the analyte concentration ranged from 1.0×10^{-6} to 1.0×10^{-3} M in all measurements.

Adsorptive stripping voltammetry experiments consisted of three stages as follows: 1) accumulation, working electrode was placed in a solution containing either the analytes or sample aliquot diluted in 0.050 M phosphate buffer (pH 7.0) for 5.0 min at open circuit potential without stirring; 2) washing, the working electrode was placed in fresh 0.050 M phosphate buffer (pH 7.0) during 0.5 min at open circuit potential without stirring; 3) measurement, the working electrode was placed in the electrochemical cell containing 0.050 M phosphate buffer (pH 7.0), and cyclic or linear sweep voltammograms were recorded as previously described. The voltammograms recorded for calibration experiments and sample analysis were background corrected using their corresponding blank signal.

Spectrophotometric measurements

Graphene dispersions, prepared as described above, were initially diluted with water to a concentration of 3.1×10^{-3} mg mL⁻¹ before the spectrophotometric measurement. The UV-visible spectra of these diluted dispersions were recorded between 200 and 800 nm using 1.0-cm quartz cuvettes.

FTIR and Raman spectroscopic measurements

Graphene oxide and reduced graphene oxide powder samples were analyzed in FTIR and Raman experiments. For this, the reduced nanomaterial was collected after washing and centrifugation and was freeze-dried. KBr pellets of the analyzed materials were prepared, and FTIR spectra were subsequently registered in the 500–4000 cm⁻¹ region (4 cm⁻¹ resolution) in the transmittance mode. On the other hand, 0.5 mg of graphene samples were affixed to glass slides by gentle pressing, and Raman spectra were subsequently recorded in the 100–4000 cm⁻¹ region (4 cm⁻¹ resolution).

High performance liquid chromatography separations

Separations were conducted in isocratic mode at 25 °C (oven-controlled) at a flow rate of 0.70 mL min⁻¹. The mobile phase consisted of 0.070 M potassium phosphate, 0.10 mM disodium salt of ethylenediamine tetraacetic acid, 1.1 mM sodium 1-octanesulfonate, 3.1 mM triethylamine, and 14 % v/v methanol, with the pH adjusted to 3.1 with citric acid [40]. The injection samples and urine samples were diluted 10000-fold and 20-fold, respectively, with the mobile phase before analysis. Both the mobile phase and diluted samples were filtered through a 0.22 μ m nylon membrane before use. Dopamine was detected

at 280 nm.

Results and discussion

Synthesis and characterization of GA-rGO

The chemical reduction of commercial graphene oxide (GO) by gallic acid was studied. GA was added to aqueous dispersions of GO in the presence of ammonia (pH 11.0) and subsequently heated at 80 °C during different durations (4.0, 6.0 y 10.0 h), as detailed in the experimental section. The reduced nanomaterial was collected after washing and centrifugation, and ultimately dispersed in pure water. For comparison, in a control experiment, the chemical reduction of GO was carried out following the same procedure, except hydrazine (HZ) was used instead of GA for 6.0 h, resulting in HZ-rGO. The reduced nanomaterials and their aqueous dispersions were characterized by spectroscopic techniques, as detailed in the measurement procedures section.

The UV-Vis absorption spectra of the GO, HZ-rGO and GA-rGO diluted dispersions were registered (Fig. S1, Supplementary Data). The UV-Vis absorption profile of GO dispersions displays a characteristic band at 230 nm ($\pi - \pi^*$ transitions of C = C bonds) and a shoulder at 310 nm ($n - \pi^*$ transitions of carbonyl groups), whereas a bathochromic shift to 269 nm is noticed in the main band of all GA-rGO obtained. This suggest that GO is reduced, and the electronic conjugation within the graphene sheets is restored upon GA-mediated reduction. Moreover, the absorption in the entire spectral region of these dispersions increases with the reaction time employed to produce each GA-rGO. This can be attributed to the efficient reduction of GO and the progressive incorporation of GA to the nanomaterial surface, resulting in a higher amount of well-dispersed material containing phenolic-related functionalities [30,32]. The spectra obtained for HZ-rGO dispersions show similar shape and present the same red-shifting in the main band, reflecting the reduction of GO. However, this dispersion displays higher absorbance values at longer wavelengths, as reflected in normalized absorbance spectra shown in Fig. S2 (Supplementary Data), which can be attributed to the light scattering effect due to the presence of larger particles, as rGO sheets tend to stack and precipitate when hydrazine is used as a reducing agent. Indeed, the absorbance values at 269 nm of these HZ-rGO dispersions decreased during the first week and solid aggregates appeared thereafter. Conversely, the reproducibility of absorbance values obtained with GA-rGO dispersions was better, as they remained disperse and stable for at least four weeks (RSD from 3.2 to 5.1 %, $n = 12$). This fact suggests the possible GA-mediated functionalization of nanomaterial during its reduction process facilitates its ultimate dispersion in water. [31,41].

FTIR spectroscopy was utilized to show the changes in some functional groups in the structure of the nanomaterial after the reduction process. Therefore, the IR spectra of commercial GO powder and reduced graphene oxide powder samples (rGO) were registered (Fig. 1A).

The FTIR spectrum of GO revealed the presence of various oxygen-containing functional groups. It exhibited bands indicating the presence of O-H bonds in hydroxyl group (3440 cm^{-1}), carbonyl bonds in both ketone and carboxylic acid groups (1726 cm^{-1}), aromatic C = C bonds vibrations (at 1630 cm^{-1}) and C-O bonds in carboxyl (1387 cm^{-1} , 1160 cm^{-1} , and 1048 cm^{-1}), epoxy (1110 cm^{-1}), and alkoxy (1048 cm^{-1}) groups. Furthermore, the C-H stretching (2960 cm^{-1} , 2918 cm^{-1} , and 2858 cm^{-1}) and bending (1460 cm^{-1} , and 1400 cm^{-1}) signals from methyl and methylene groups can be observed. After chemical reduction, changes in the spectra profile were observed. The band near 1630 cm^{-1} disappeared for all rGO by GA, whereas a new band centered at 1578 cm^{-1} was observed in all cases, displaying higher absorbance for longer reaction time. The same effect was observed in HZ-rGO material. The presence of this band is attributed to the red shifting of C = C group stretching signal when increasing conjugation within the graphene sheet, suggesting the progressive chemical reduction of GO and

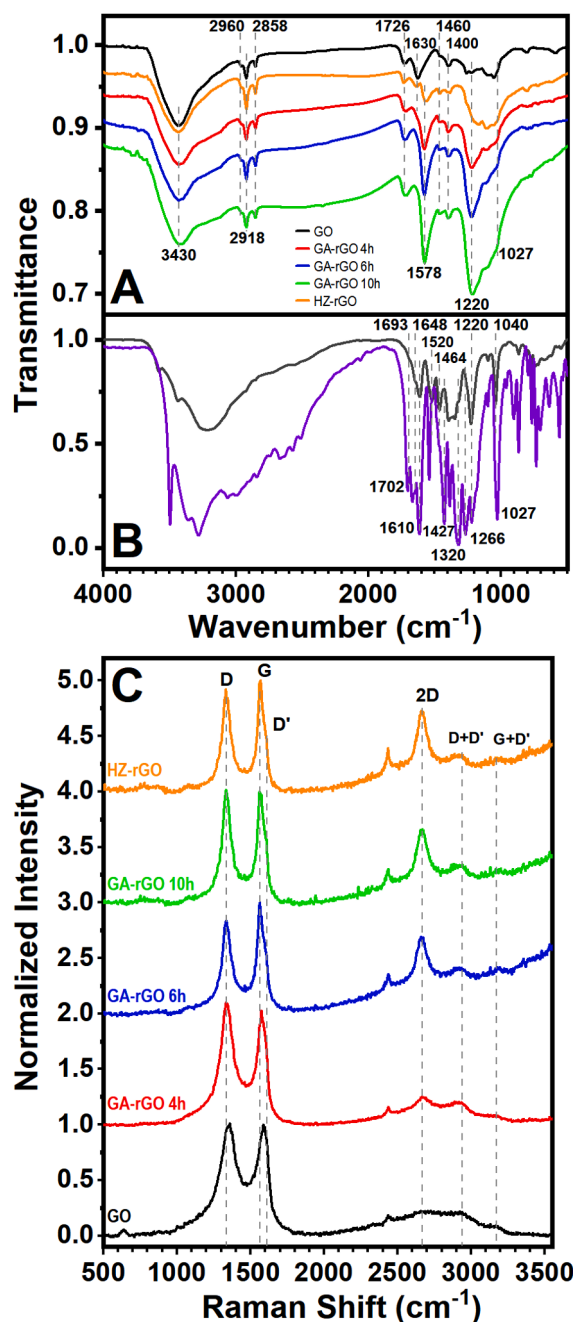


Fig. 1. (A) FTIR spectra of different powder nanomaterial: GO (—), HZ-rGO (—), and GA-rGO prepared at different reaction time: 4.0 h (—), 6.0 h (—) and 10.0 h (—); (B) FTIR spectra of GA (—) and supernatant material (—) obtained after reduction of GO with GA during 6.0 h; (C) Raman spectra of different powder nanomaterial: GO (—) and rGO by HZ (—), and GA prepared at different reaction time: 4.0 h (—), 6.0 h (—) and 10.0 h (—). Raman intensities are normalized to G-band. FTIR and Raman spectra have been vertically displaced for the sake of clarity.

restoration of sp^2 domains [42]. This could be the reason why the carbonyl stretching signal of rGO by GA appears at 1718 cm^{-1} . Nonetheless, signals of oxygen functional groups in the $1300\text{--}900\text{ cm}^{-1}$ range were not removed, as could be expected. Indeed, rGO by GA exhibited some absorption bands even stronger than those of GO, whose intensity increases with the elapsed reaction time. In fact, strong absorption bands

can be noticed in the same region of the FTIR spectra of GA and the supernatant reaction products obtained after GO reduction by GA during 6.0 h, as displayed in Fig. 1B. This fact could confirm the functionalization of the nanomaterial during the reduction process, by chemical or physical interaction between the already existing groups and the new ones generated during this process. The broadening of hydroxyl stretching band in the range $3400\text{--}3000\text{ cm}^{-1}$ to lower wavenumbers could be attributed to the incorporation of structures with O-H bonds within rGO, in accordance with those signals observed in both supernatant and GA spectra. The increasing occurrence of hydroxyl groups promotes intermolecular hydrogen bonding, thereby additional broad bands start to appear at these frequencies (note that this band broadening was not displayed by rGO produced with HZ). In addition, the increase in the absorbance and width of the band centered at 1220 cm^{-1} , associated to C-O stretching and O-H bending vibrations of phenol groups, confirms the presence of these groups in the nanomaterial [43]. It is widely assumed that GA oxidation proceeds through formation of a phenolate radical and subsequent evolution to quinone structures, whereas in some circumstances, the formation of dimers and polymers through ester and ether bridges [44] or C-C linkage [45] has been suggested. The inspection of the supernatant reaction products spectra suggests the presence of quinone groups, as supported by the presence of a new carbonyl band at 1648 cm^{-1} (Fig. 1B), which appeared between C = O (1693 cm^{-1}) and C = C stretching (1610 cm^{-1}) signals of carboxylic group and aromatic ring (these bands are displayed by GA at similar wavenumber). The absence of signals in the $1750\text{--}1710\text{ cm}^{-1}$ region can be interpreted like ester bonds were not generated during GA oxidation, neither in the nanomaterial nor reaction solution. Other aromatic C = C stretching bands can be observed at 1520 and 1464 cm^{-1} . The 1450 to 1000 cm^{-1} range is characterized by multiple bands from C-O stretching and O-H bending vibrations, which are combined and/or overlap in-plane C-H bending and other aromatic ring vibration modes, thereby they cannot be properly assigned. In addition, several reaction products, as well as parent GA might constitute the obtained supernatant material. However, the weakening or vanishing of strong signals observed for GA at 1427 , 1320 , and 1266 cm^{-1} reflects changes in the structure and distribution of phenolic moieties after the reaction with GO. Moreover, the bands observed at 1220 and 1027 cm^{-1} , usually assigned to C-O stretch of phenol groups in GA, are retained in the supernatant spectra (the last band is blue shifted to 1040 cm^{-1}) thus it can be cautiously stated that products still contain many of these functionalities. The presence of aromatic ether linkages in the reaction products cannot be demonstrated since the C-O-C symmetric and asymmetric stretching signals at 1250 and 1050 cm^{-1} are not clearly shown. However, the supernatant spectra display many weak signals at wavenumbers below 1400 cm^{-1} , especially in the 900 to 400 cm^{-1} range, where aromatic ring and C-H in-plane and out of plane vibrations, as well as other secondary vibration modes of oxygen groups, reveal their signals. Therefore, the possible formation of polymeric units either through ether or C-C bonding cannot be ruled out. Finally, from the comparison of these spectra to that obtained for rGO produced with GA, particularly at wavenumbers below 1200 cm^{-1} , it cannot be assured among GA or any reaction product which one was getting adsorbed during the GO reduction and functionalization.

The same materials studied by FTIR were further characterized by Raman spectroscopy. These spectra (Fig. 1C) displayed three main bands, which are present in graphitic-like carbon nanomaterials such as carbon nanotubes and graphene [46–49] namely, the G-band, around 1565 cm^{-1} , the D-band, around 1335 cm^{-1} , and the 2D-band, around 2670 cm^{-1} . The G-band results from the well-ordered sp^2 graphitic sheet (i.e., crystallinity of the sample, pristine arrangement of atoms), whereas the D-band is related to structural disorder (defects) in the graphitic structures, the sp^3 carbon, and other impurities. The 2D peak (also called G' in the literature) is referred to as the second order overtone of the D-band and is indicative of long-range order in a sample. Other minor features present in these spectra are the D' , $\text{D} + \text{D}'$ and $\text{G} +$

D' signals. The D' -band which is a weak shoulder of the G-band at higher frequencies (around 1610 cm^{-1}), is also a double resonance feature induced by disorder and defects. The second-order peaks around 2940 cm^{-1} ($\text{D} + \text{D}'$) and 3175 cm^{-1} ($\text{G} + \text{D}'$) are combination modes of either D or G bands with D' bands. These bands are considered to be defect-activated, and their origin is related to defects in the graphenic layers, as well as edge-plane sites in the sheet borders, the number of layers in graphite/graphene particles, and their stacking, or even surface curvature [48]. The spectra obtained from parent GO displays broad D- (1352 cm^{-1}) and G- (1598 cm^{-1}) bands with similar peak intensity, as well as weak and broad second order bands (above 2000 cm^{-1}). This is indicative of a highly disordered carbon material with distinct size domains due to disrupting sp^2 structure and functionalization acquired during GO production. The spectra of materials produced after GA treatment present downshifted and narrower D- (1332 cm^{-1}) and G- (1565 cm^{-1}) bands, with alleviated interband distortion [50], suggesting a less disordered sp^2 structure and a more uniform size distribution of ordered domains. The D-to-G intensity ratio value ($I_{\text{D}}/I_{\text{G}}$) slightly increases from 0.97, estimated in GO, to 1.10 after 4.0 h of treatment and then decreases to 0.90–1.00 in materials treated for a longer time. This is consistent with a transition from fully disordered sp^2 material to nanocrystalline graphite, according to the stages of amorphization trajectory described by Ferrari [51]. Therefore, the reduction process allowed the formation of nanocrystalline rGO, with structural defects mostly related to edges and C-H ending of the sp^2 network, whereas vacancies or kinks generated in carbon hexagons after the removal of oxygenated groups needed further treatment to be fixed [52]. The apparition of a well-defined 2D-band at $2665\text{--}2670\text{ cm}^{-1}$, especially in those materials treated for 6.0 and 10.0 h, can be another symptom of the restoration of the graphenic interatomic structure. The shape and intensity of this band are associated with the number of graphene layers and the three-dimensional ordering of the material [53], as well as the presence of dopant agents in the nanomaterial structure [54], and the purity of samples [46]. The spectra of rGO obtained using HZ is characterized by the D- (1332 cm^{-1}), G- (1568 cm^{-1}), and 2D-bands (2665 cm^{-1}), whose position, width and intensity are very similar to those shown by GA-treated material for 6.0 and 10.0 h. Therefore, the reducing ability of GA promotes the restoration of the graphitic lattice of the oxidized nanomaterial and effectively produces rGO with a comparable nanographitic structure to that provided by HZ. Moreover, the similarity of the spectra profile suggests that incorporation of phenolic groups to rGO produced by GA was achieved through non-covalent interactions, whereas covalent bonding would induce to distinctive spectral changes in the first order interband region as well as in the D-to-G and 2D-to-G intensity ratios [48,50,54].

The morphological characterization of the dried films of the nanomaterials obtained after deposition of the dispersions onto a glassy carbon support was performed by FE-SEM. Fig. 2 shows the bare support surface without any modification (A) and modified with GO (B), HZ-rGO (C) and GA-rGO (D-F) dispersions. The bare support shows high roughness highlighting the sharp edges of well-packed graphitic layer structures of different sizes. The GO modified surface exhibits a thin layer of wrinkled sheets with stacked edges non uniformly distributed upon the support, where the underlying graphitic edges can be seen in the less densely covered areas. After the reduction process of the nanomaterial, the degree of graphene sheets' packing decreases, showing thinner layers with a structure similar to crumpled silk. In the images obtained with the HZ-rGO and GA-rGO dispersions (4.0 h), the morphology of the support is yet visible, but in the case of the GA-rGO dispersions (6.0 and 10.0 h), a smooth, homogeneous, and completely coated surface is observed. This restructuring of graphene sheets in these films is possibly promoted by the better dispersion of the nanomaterial facilitated by the adsorption of phenolic substances on its surface.

Microscopy experiments were complemented by energy dispersive X-ray analysis (EDX) of the surface covered with nanomaterials. The

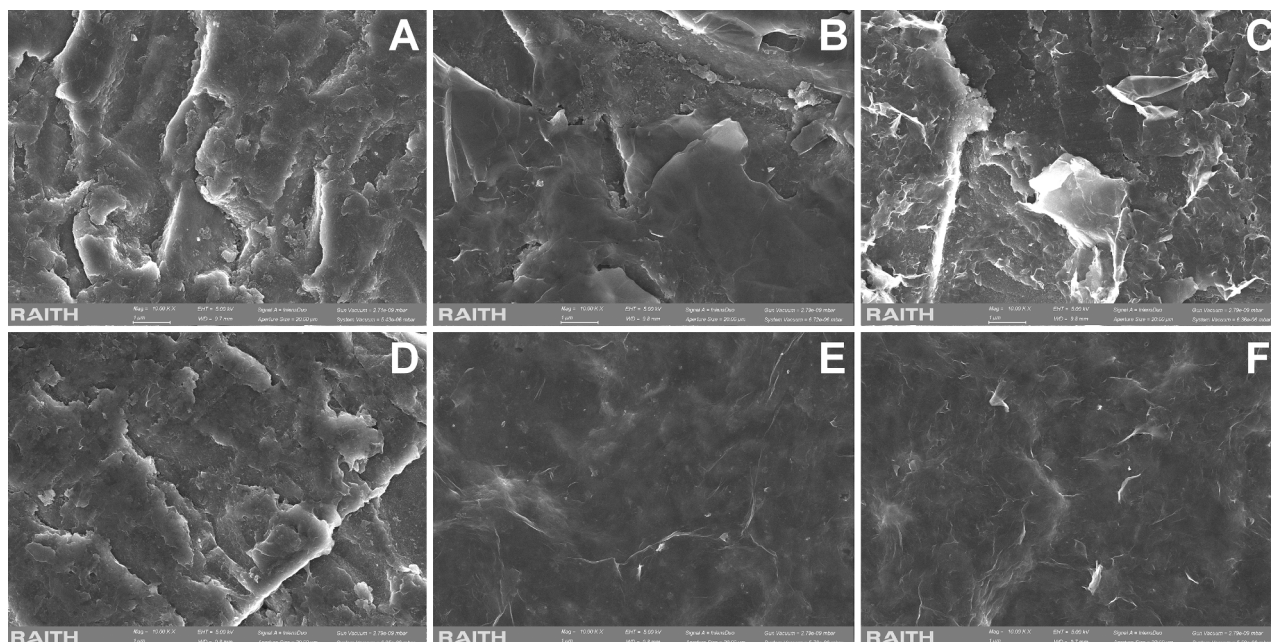


Fig. 2. FE-SEM micrographs of the bare glassy carbon support (A) and modified with dispersions of GO (B), HZ-rGO (C), and GA-rGO prepared at different reaction time: 4.0 h (D), 6.0 h (E) and 10.0 h (F); Acceleration voltage: 5.0 kV. Magnification: x10000.

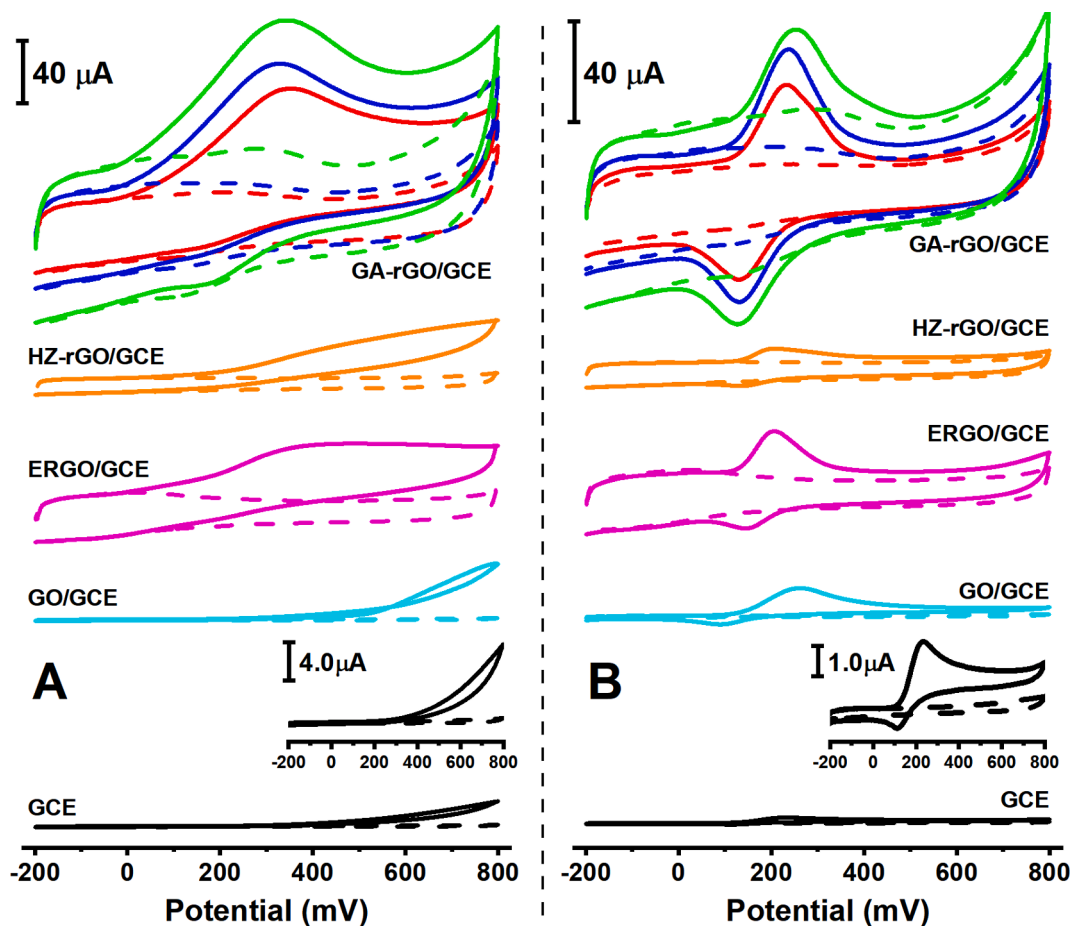


Fig. 3. Cyclic voltammograms of 1.0×10^{-3} M hydrazine (A) and 1.0×10^{-4} M dopamine (B) obtained at GCE, HZ-rGO/GCE, ERGO/GCE and GCE modified with GA-rGO dispersions prepared at different reaction time: 4.0 h (—), 6.0 h (—) and 10.0 h (—). Supporting electrolyte: 0.050 M phosphate buffer of pH 7.0. Scan rate: 0.050 V s^{-1} . All electrodes were previously pretreated by performing 10 scans in supporting electrolyte. Background voltammograms are shown in dashed lines.

elemental composition derived from EDX spectra (Supplementary Data, Table S1) reveals that the C/O atomic ratio of HZ-rGO was higher than that shown by GO, indicating the removal of oxygen atoms because of the nanomaterial reduction. Additionally, the C/O atomic ratio of GA-rGO obtained after 4.0 h is comparable to that shown by HZ-rGO, suggesting a similar reduction degree of GO. For a longer reaction time, the C/O atomic ratio of GA-rGO materials decreases due to the incorporation of oxygen atoms from the adsorbed phenolic groups, in agreement with FTIR results.

Electrochemical activity of modified electrodes (GA-rGO/GCE)

The rGO materials produced by either GA and HZ reducing agents were incorporated onto the GCE surface, and the electrochemical performance of such modified electrodes was examined by cyclic voltammetry (CV) towards HZ and DA. To conduct this study, GCEs were modified with 5.0 μL of each GA-rGO dispersion (GA-rGO/GCE), previously diluted in water (1:4 dilution factor, 0.50 mg mL^{-1} of nanomaterial). Furthermore, GCE modified with 5.0 μL of each GO (GO/GCE) and HZ-rGO (HZ-rGO/GCE) dispersion, as well as an electrochemically-reduced graphene oxide electrode (ERGO/GCE), were prepared for control experiments. All electrodes underwent a voltammetric electrochemical pretreatment (as described in experimental section) to establish a stable background voltammogram before recording the response in the presence of each analyte. Fig. 3A displays cyclic voltammograms of the different electrodes obtained at 0.050 V s^{-1} in a 0.050 M phosphate buffer solution of pH 7.0, both in the absence and presence of 1.0 $\times 10^{-3}$ M HZ.

No oxidation peak for HZ was observed in the voltammograms at both bare GCE and the GO/GCE. Instead, a progressive increase in the current was noticed at potentials higher than 200 mV, up to 800 mV. The voltammetric behavior observed at rGO electrodes was quite different. A well-defined oxidation wave was observed, with onset potentials of +150 mV for HZ-rGO/GCE, +50 mV for ERGO/GCE and 0 mV for GA-rGO/GCEs. This difference can be attributed to the presence of a high density of edge-plane sites, as well as oxygenated species such as carbonyl and hydroxyl groups, which promote a faster electronic transfer rate. For example, the background voltammograms obtained with GA-rGO/GCEs exhibited clear anodic and cathodic signals with higher currents. In contrast, when HZ was present, its oxidation wave appeared at a significantly lower overpotential. This fact could be ascribed to the specific oxygenated species generated during the chemical reduction process and subsequently incorporated into the nanomaterial surface. Therefore, the proposed synthesis of GA-rGO promotes a controlled functionalization of the nanomaterial enriched with oxygenated functional groups. This is in accordance with the results shown by FTIR, ultimately giving rise to the catalytic oxidation of hydrazine and the improved voltammetric signals observed at GA-rGO/GCE. This favored electrochemical response is not surprising, as it is well-known that the electrochemistry of HZ benefits from the presence of carbonyl groups on the electrode surface [55]. Furthermore, the enhanced electrochemical performance of GCE modified with reduced graphene oxide in the oxidation of this compound has been reported and attributed to the presence of edge-plane sites in this nanomaterial [56]. Additional support for this idea can be found in the voltammograms conducted in blank supporting electrolyte to reduce GO/GCE and generate ERGO/GCE (Fig. S3A in Supplementary Data). These voltammograms are characterized by the presence of a broad irreversible wave at ca. -0.90 V in the first cathodic scan, which progressively disappears in subsequent scans as ERGO is produced [16]. However, such a wave was not observed under the same experimental conditions for GA-rGO/GCE or HZ-rGO/GCE. This cathodic signal comprises multiple reduction processes involving different oxygen functional groups within the GO structure, whose assignation is not straightforward. It is generally assumed that when using neutral buffers, the electrochemical reduction of epoxy, peroxy or aldehyde [16], as well as hydroxyl and, in some

extent, carbonyl groups [57] in GO (typically located in the basal plane), occurs at relatively more anodic potentials than other groups like carboxyl, ester, and isolated carbonyl (usually placed in the edge plane) [16,58]. The removal of epoxy and peroxy groups from GO is linked to the enhancement in the electrochemical performance of rGO based electrodes [16,58] and can elucidate the disparity between GO/GCE and ERGO/GCE responses towards HZ. These oxygenated functionalities were efficiently eliminated during the chemical reduction of GO by either GA and HZ, as evidenced by the absence of cathodic wave in the -0.6 to -1.1 V range at GA-rGO/GCE or HZ-rGO/GCE (Fig. S3B in Supplementary Data). Moreover, carbonyl and hydroxyl groups should be present in these materials, as evidenced by the negative shift of the HZ oxidation wave at HZ-rGO/GCE and, especially, GA-rGO/GCE. Therefore, the electrochemical reduction of these groups could be the reason why HZ-rGO/GCE and GA-rGO/GCE display higher cathodic currents in the -1.2 to -1.4 V range [57].

Further voltammetric experiments were conducted in the absence and the presence of 1.0×10^{-4} M DA using the same supporting electrolyte, and representative cyclic voltammograms (0.050 V s^{-1} scan rate) are shown in Fig. 3B. These CVs displayed an anodic wave in the first scan coupled to a cathodic one in the reverse scan, a typical quasi-reversible behavior that characterizes the DA redox system. The electrodes modified with rGO provided higher voltammetric signals, both faradaic and capacitive, combined with lower overpotentials and smaller peak-to-peak separation potentials (ΔE_p) than those shown by bare GCE or GO/GCE (Supplementary Data, Table S2). In fact, GCE and GO/GCE presented ΔE_p of 122 ± 4 and 174 ± 9 mV, respectively, whereas 57 ± 4 mV and 70 ± 6 mV were shown at ERGO/GCE and HZ-rGO/GCE. Furthermore, 88 ± 18 mV, 103 ± 8 mV, and 130 ± 7 mV were observed at GA-rGO/GCEs, respectively. Additionally, the anodic-to-cathodic peak current ratio evaluated at GA-rGO/GCEs electrodes ranged from 1.4 to 1.6, closer to the expected value of 1 for reversible systems, whereas values higher than 2 were calculated for the other modified electrodes and bare GCE. Therefore, all these values demonstrate that the presence of these rGO materials on the electrode surface clearly improves the electron-transfer kinetic of DA redox system. Moreover, the increase in intensity and symmetry of DA waves displayed by the different GA-rGO/GCE suggests strong adsorption of the compound on these surfaces due to the presence of both edge-plane defects and, especially, oxygen-containing functional groups generated during the GO reduction process driven by GA. Indeed, the π - π stacking based interactions between DA and the basal plane of graphene dominate the electrochemical activity of graphene based electrochemical sensors towards DA, and a selective adsorption behavior toward DA has been reported [59]. In addition, the functionalization of graphene with oxygen-containing functional groups enhances the electrochemical transfer kinetics as well as the catalytic activity for the electrochemical oxidation of DA. This catalytic effect has been attributed to the presence of hydrogen bonding sites on the graphene surface, which assisted DA oxidation by transient bonding to hydrogen located in its catechol moiety, thus leading to "proton-assisted electron transfer". Additionally, the presence of anionic oxygenated groups could favor the selective determination of DA in presence of interferents like ascorbate, due to electrostatic interactions with the anionic surface [60,61].

Regarding the electrodes modified with GA-rGO materials, all of them have exhibited promising potential for the electroanalysis of both HZ and DO; however, their performance is linked to the reaction time applied for the synthesis of rGO. Indeed, an increase in both the faradaic (I) and capacitive (C) currents was observed when the electrode was modified with dispersions of GA-rGO obtained at longer reaction times. Nevertheless, the I/C ratio was similar for those materials obtained using 4.0 and 6.0 h and decreased for the 10.0 h material, whereas a wider ΔE_p of DA waves was observed as well. Therefore, the reaction time given for GO reduction has an important effect on the functionalization of the nanomaterial and its subsequent electrochemical response. Consequently, the GA-rGO material obtained using a 6.0 h reaction time was

selected for further studies henceforth since it offers a favorable I/C ratio, combined with high sensitivity and low overpotentials. The effect of the amount of nanomaterial employed to obtain the film on its electrochemical performance was considered next. Therefore, dispersions of the selected GA-rGO material, containing 0.50; 0.33, and 0.20 mg mL⁻¹ were prepared from the former concentrated dispersion by suitable dilution (1:4, 1:6 and 1:10 factor) in water. Subsequently, GCE were modified with 5.0 μ L of these dispersions, and the resulting electrodes were evaluated by CV using 1.0×10^{-3} M FC and 1.0×10^{-4} M DA in a 0.050 M phosphate buffer solution (pH 7.0), as before. The voltammetric response of these surfaces resulted in a decrease in both I and C currents but an increase in the I/C ratio (Supplementary Data, Table S3) when decreasing the amount of deposited material (dispersions of lower concentration). Indeed, GA-rGO/GCE prepared with 0.20 mg mL⁻¹ dispersions displayed I and C ca 30 and 65 % lower, respectively, than those observed using electrodes prepared with 0.50 mg mL⁻¹ dispersions. Similarly, I and C were ca 20 and 50 % lower, respectively, when using electrodes modified with 0.33 mg mL⁻¹ dispersions. However, the I/C ratio was twice higher at electrodes modified with diluted dispersions, without remarkable changes in onset potential, peak potential, and ΔE_p . Therefore, the 0.20 mg mL⁻¹ concentration of nanomaterial (1:10 dilution factor) was used in subsequent experiments.

The electrochemical performance of the GA-rGO/GCE toward other interesting compounds was examined. For this purpose, potassium ferricyanide (FC), uric acid (UA) and ascorbic acid (AA) were employed. The cyclic voltammograms of 1.0×10^{-3} M solutions of FC and AA and 1.0×10^{-4} M solution of UA in 0.050 M phosphate buffer solution with a pH 7.0 were obtained at GA-rGO/GCE, GO/GCE and at the naked GCE and are summarized in Fig. 4.

The anodic waves of both AA and UA, corresponding to their irreversible electrochemical oxidation, and the typical redox couple of FC reversible system were displayed in all cases. Nevertheless, GCE modified with the GA-rGO layer provided signals at lower overpotential than that observed at the other electrodes, with a negative shift of 153 mV and 40 mV for AA and UA, respectively, and a decrease of 45 mV in ΔE_p of FC, in comparison to the bare GCE. In fact, heterogeneous electron transfer rate constants (k^0) for the FC redox system were estimated using such ΔE_p , following Lavagnini's work [62] and values of 1.4×10^{-3} , 1.6×10^{-4} , and 6.5×10^{-4} cm s⁻¹ were calculated for GA-rGO/GCE, GO/GCE, and GCE, respectively. These results suggest that films prepared with GA-rGO dispersion provide better electrical conductivity and enhanced electron transfer. In addition, AA and FC peak currents at GA-rGO/GCE were only slightly higher than those shown at bare GCE, whereas GO/GCE displayed weaker signals. However, a noticeable sharp and symmetric UA wave was observed at GA-rGO modified electrodes, exhibiting a 4-fold increase in its anodic current when compared to the other

electrodes. This fact suggests that UA could be specifically adsorbed on the GA-rGO/GCE.

In view of the results achieved and exposed along this section, the GA-rGO materials (and their dispersions) possess structural properties that enable the successful modification of GCE. These modified electrodes have demonstrated unique electrochemical performance towards the tested compounds, especially DA, which could be leveraged for electroanalytical purposes.

Adsorptive stripping voltammetry of DA and UA using GA-rGO/GCE

Electrochemical studies were conducted to confirm the adsorption phenomenon of DA on GA-rGO/GCE using an adsorptive stripping scheme. Fig. 5A displays cyclic voltammograms obtained either at GA-rGO/GCE, GO/GCE, and bare GCE in a blank 0.050 M phosphate buffer solution pH 7.0 after a 5.0 min exposition to a 1.0×10^{-5} M DA solution in 0.050 M phosphate buffer at pH 7.0, at open circuit potential. The voltammograms of GA-rGO/GCE exhibited a pair of well-defined redox peaks with sharp and symmetric shape. The anodic and cathodic currents were ca. 10 and 6 μ A, respectively, and their ΔE_p was 61 mV. In contrast, no DA signals were observed at GCE, while the anodic and cathodic currents at GO/GCE were substantially smaller (10-fold lower), along with a 48 mV-increase in ΔE_p . The comparison with the data obtained using direct voltammetric measurements at GA-rGO/GCE revealed an enhancement in the sensitivity of the anodic peak (from 0.27 to 0.90 μ A μ M⁻¹) by introducing the accumulation step, with lower peak potential and smaller ΔE_p , typical of adsorption-controlled electrochemical processes. These results clearly demonstrated the advantages of the presence of GA-rGO materials on the electrode surface in the adsorption and subsequent electrooxidation of DA.

Considering this efficient adsorption of DA at GA-rGO/GCE, we developed a strategy for the quantification of DA based on Adsorptive Stripping Voltammetry (AdSV) with medium exchange. In this approach, DA accumulation at open circuit potential for durations ranging from 60 to 600 s was examined using an accumulation solution containing 1.0×10^{-5} M DA in supporting electrolyte. Voltammograms recorded in blank supporting electrolyte exhibited the anodic and cathodic waves of adsorbed DA, which gradually increased for an accumulation time from 60 to 300 s, with only slight changes observed for longer times (Fig. S4 in Supplementary Data). Therefore, the maximum adsorption capacity of DA onto the GA-rGO/GCE surface under these conditions was attained at ca. 300 s. Subsequently, the accumulation potential was investigated by applying potentials ranging from -200 to 0 mV for 5.0 min in the same accumulation solution. No improvements in DA voltammetric signals were observed in these experiments, and the highest sensitivity was obtained at open circuit.

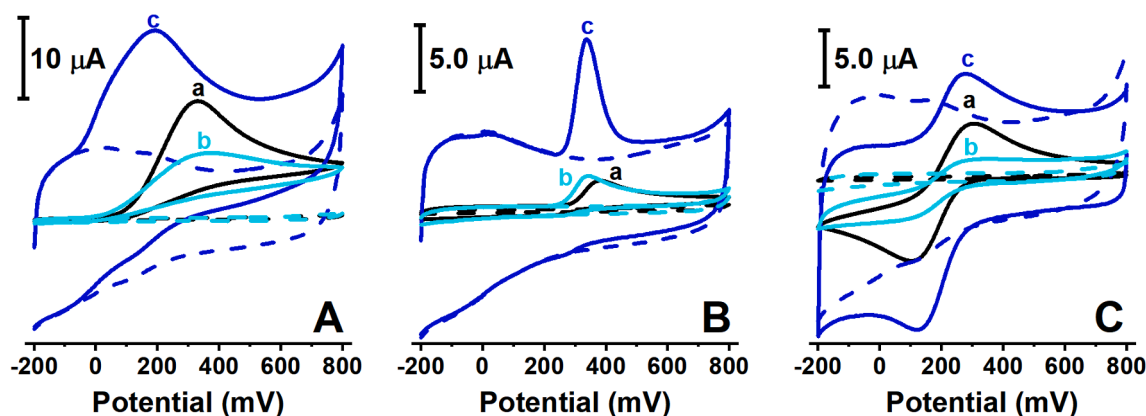


Fig. 4. Cyclic voltammograms of ascorbic acid (A), uric acid (B) and potassium ferricyanide (C) obtained at GCE (—; a), GO/GCE (---; b) and GA-rGO/GCE (····; c) electrodes. Supporting electrolyte: 0.050 M phosphate buffer of pH 7.0. AA and FC concentration: 1.0×10^{-3} M, UA concentration: 1.0×10^{-4} M. Other conditions as in Fig. 3.

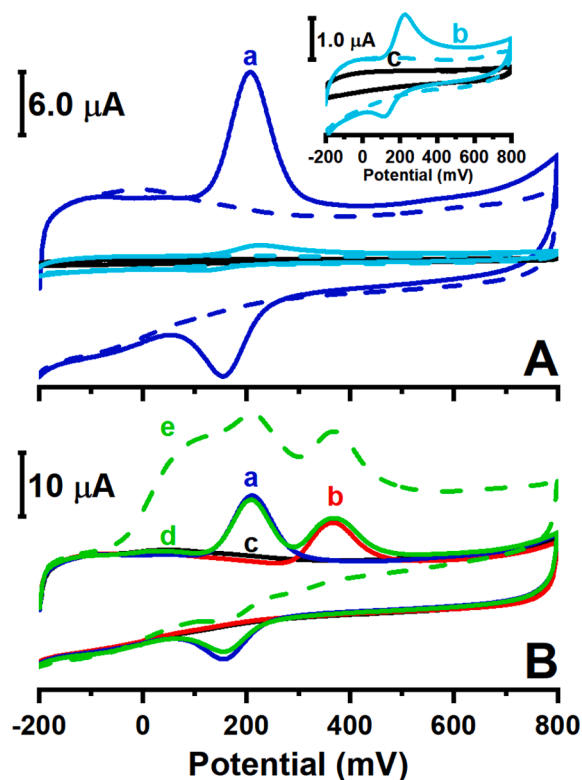


Fig. 5. (A) Stripping voltammograms obtained at the GA-rGO/GCE (—; a), GO/GCE (—; b) and GCE (—; c) after accumulation in 1.0×10^{-5} M DA. Background voltammograms are shown in dashed lines. Inset shows the magnified stripping voltammograms obtained using GO/GCE and GCE. (B) Stripping voltammograms obtained at the GA-rGO/GCE after accumulation in solutions containing: 1.0×10^{-5} M DA (—; a), 1.0×10^{-4} M UA (—; b), 1.0×10^{-4} M AA (—; c), mixed solution of the three compounds in the same concentration as the individual solutions (—; d). Cyclic voltammogram for direct measurement of the mixture solution is shown in green dashed line (—; e). Accumulations conditions in (A) and (B): 5.0 min at open circuit potential without stirring using 0.050 M phosphate buffer solution of pH 7.0 as supporting electrolyte. Measuring conditions in (A) and (B): fresh 0.050 M phosphate buffer solution of pH 7.0 and 0.050 V s⁻¹ scan rate. (For interpretation of the references to colour in this figure legend, the reader is referred to the web version of this article.)

Therefore, 5.0 min at open circuit potential was selected as the optimum adsorption conditions for further studies. Following, DA solutions ranging from 5.0×10^{-7} M to 5.0×10^{-5} M were subjected to AdSV (Supplementary Data, Fig. S5A), and the corresponding calibration plot exhibited a linear relationship between oxidation peak current and DA concentration up to 2.0×10^{-5} M, with a sensitivity of $(0.90 \pm 0.02) \mu\text{A } \mu\text{M}^{-1}$ (Supplementary Data, Table S4). A detection limit of 0.09 μM (taken as $3s_b/S$, where s_b is the standard deviation of the blank signal, and S is the sensitivity) and a quantification limit of 0.3 μM (taken as $10s_b/S$) were obtained.

Some experiments were subsequently conducted to study the reproducibility, repeatability, and stability of GA-rGO/GCE for the AdSV of DA. Initially, the impact of the electrode preparation process on the reproducibility was evaluated by examining the AdSV signals of a 2.0×10^{-6} M DA solution. This involved six different electrodes modified with the same dispersion and an additional set of nine electrodes modified with three different dispersions. The calculated Relative Standard Deviation (RSD) value using the DA peak current from electrodes prepared with the same dispersion was 5.1 % ($n = 6$), whereas for different dispersions, it was 7.9 % ($n = 9$). Therefore, the preparation process does not introduce large variability to DA quantification. Subsequently, eight

consecutive AdSV experiments were performed with the same modified electrode in a 2.0×10^{-6} M DA solution to assess repeatability. The voltammograms obtained during the three initial experiments displayed well-defined DA signals, with peak current variability giving RSD values of 8.3 %. However, distorted waves were observed in subsequent experiments, accompanied with peak potential shifting and difficulties in baseline evaluation, which introduced significant variability in peak current values. Therefore, exhaustive reusability of the electrode is hindered, and using fresh modified electrodes is recommended to reduce variability. The long-term storage stability of GA-rGO/GCE was evaluated by monitoring the response to 2.0×10^{-6} M DA solutions from different electrodes stored in a dry environment after their preparation. The voltammetric peak currents of electrodes stored for up to 9 days retained more than 90 % of the initial current without noticeable peak potential shifting. However, weaker, and distorted voltammetric waves were observed for longer storage times.

Bearing in mind that AA and UA are important interferents in the electrochemical quantification of DA, their adsorption onto GA-rGO/GCE was evaluated through AdSV experiments performed at open circuit potential after 5.0 min accumulation in AA and UA solutions, each at a concentration of 1.0×10^{-4} M (Fig. 5B). The CV obtained in a 0.050 M phosphate buffer solution after accumulation in the AA solution did not show any peak; therefore, the adsorption of AA was negligible under these experimental conditions. On the other hand, a well-defined anodic peak at 364 mV was observed when accumulation was carried out in UA solution, demonstrating the adsorption of UA at GA-rGO/GCE. As can be seen in Fig. 5B, the AdSV analysis of a mixed solution containing the three compounds at the same concentration showed a CV that corresponds to the sum of the voltammograms corresponding to the individual analysis of each compound. This indicates the possibility of simultaneous determination of DA and UA in the presence of AA. However, this determination was not possible without the previous accumulation step because the AA signal overwhelmed the DA and UA signals, preventing any independent quantification of the three species.

This behavior is related to the intermolecular interaction of analytes with the functional groups of the electrode material. The adsorption and electrochemical processes of DA on graphene materials are favored by the multiple interactions promoted by the amine, hydroxyl, and aromatic groups within this molecule. These interactions can be summarized as follows [63]: (i) π - π interactions between the aromatic moieties of DA and graphene, (ii) H-bonding between the amine and hydroxyl groups of DA and the oxygenated substituents in graphene surface (carboxylic, carbonyl, hydroxyl, or epoxy), (iii) cation- π interactions between the protonated amine group of DA and the aromatic moieties of graphene, and (iv) electrostatic interactions between the protonated amine group of DA and the carboxylate groups of graphene (DA is mainly in its cationic form under these pH conditions; pK_a 8.87). The introduction of phenolic groups in the GA-rGO material increases the occurrence of polar and H-bonding interactions, thus promoting DA adsorption and facilitating its electrochemical oxidation [60,61]. Regarding UA and AA, these molecules have low delocalized π electron density, especially AA. In addition, at pH 7.0 both exists in their anionic forms, urate (pK_a 5.7) and ascorbate (pK_a 4.10). Therefore, their π - π interactions with graphene are weaker than those expected for DA, and they experience electrostatic repulsion with the negatively charged functional groups of graphene material. Both urate and ascorbate can undergo H-bonding with the carboxyl and hydroxyl moieties of GA-rGO, through their neutral =NH and -OH groups, respectively. The cumulative effect of such interactions can enhance UA and AA electrochemical processes but are not sufficiently important to promote their adsorption. Therefore, UA accumulation in the electrode surface is limited compared to DA whereas AA do not exhibit adsorptive properties.

The AdSV of DA solutions of different concentrations in the presence of both AA and UA, each at a concentration of 1.0×10^{-4} M, was carried out under the selected conditions (Supplementary Data, Fig. S5B). The

corresponding calibration plot of the DA signal derived from these mixtures displayed a similar linear range, with a sensitivity value ($0.86 \pm 0.03 \mu\text{A } \mu\text{M}^{-1}$) very close to the one obtained before for DA alone (Supplementary Data, Table S4). Statistical comparison of the slopes of the two regression lines showed no significant difference between them (Supplementary Data, Table S5). This result confirms that GA-rGO/GCE allows the highly selective determination of DA in the presence of an excess of AA and UA. On the other hand, the AdSV response to an increasing concentration of UA in the range of 1.0×10^{-5} to 1.0×10^{-4} M, either in the presence or absence of 5.0×10^{-6} M DA, was also studied (Supplementary Data, Fig. S5C & D). In both cases, the anodic signals corresponding to UA showed a correlative increasing with the UA concentration throughout the studied range, and no significative differences were observed in the sensitivity obtained, with values of (0.059 ± 0.004) and (0.056 ± 0.003) $\mu\text{A } \mu\text{M}^{-1}$ in the absence and presence of DA, respectively (Supplementary Data, Tables S4 & S5). These results confirmed the ability of GA-rGO/GCE for the simultaneous determination of DA and UA by AdSV.

Analytical applications

The proposed GA-rGO/GCE was tested for the determination of DA in a medication product (Dopamine hydrochloride injections) and for the determination of DA and UA in human urine samples. Five samples of dopamine hydrochloride injections (200 mg / 5mL) were properly diluted with 0.050 M phosphate buffer of pH 7.0 and setting the DA concentration to 2.1×10^{-6} M (10^5 dilution factor) and subjected immediately to AdSV. The standard addition method (two 2.0 μM additions were made) was used for DA determination (Representative stripping voltammograms can be found in Supplementary Data, Fig. S6). A linear relationship was observed between the variation of anodic peak current versus added DA concentration in these experiments, with sensitivity values ranging from 0.88 to $1.08 \mu\text{A } \mu\text{M}^{-1}$. A DA content of $2.2 \pm 0.2 \times 10^{-6}$ M ($n = 5$) (expressed as mean \pm SD, and equivalent to $2.1 \pm 0.2 \times 10^2$ mg of dopamine hydrochloride in 5 mL of injection) was evaluated in this manner, in good agreement with the expected value of dopamine hydrochloride in the analytical sample (One-sample Student's t -test: $t_{\text{cal}} = 1.57 < t_{\text{crit}} = 2.78$, for a significance level of 5 %, 4 degrees of freedom and 2 tails). Similarly, a DA content of $2.07 \pm 0.09 \times 10^2$ mg

of dopamine hydrochloride in 5 mL of injection ($n = 3$) was evaluated through chromatographic analysis.

For the determination of UA in human urine, all the samples were 200-fold diluted with the supporting electrolyte before AdSV analysis. Their corresponding voltammograms displayed one anodic peak at ca. + 360 mV, which could be attributed to the UA signal. In fact, the addition of UA to these diluted samples resulted in an increase of this peak (Fig. 6A). These signals were used to evaluate UA concentration in all these test solutions using external calibration equation, and the results are displayed in Table S6. The concentration values found showed RSD ranging from 3.5 to 5.9 % ($n = 3$), and the subsequently calculated recoveries ranged from 82 to 104 %, with an average value of 93 %. Ultimately, the UA content obtained in urine samples was $81 \pm 3 \text{ mg dL}^{-1}$ (mean \pm SD; $n = 3$) which was in good agreement with $86 \pm 5 \text{ mg dL}^{-1}$ (mean \pm SD; $n = 3$), as evaluated with an enzymatic-colorimetric test kit for UA (Randox UA 230). Therefore, this AdSV-based determination of UA in urine is sufficiently reliable and reproducible, and no matrix interference was evidenced in light of these results.

With the aim of detecting the presence of DA in urine, both whole and DA spiked (40 μM level) samples were 20-fold diluted in supporting electrolyte and subsequently analyzed by AdSV. Representative voltammograms are depicted in Fig. 6B, where the DA signal was observed at ca. + 210 mV, specifically in spiked samples. It is noteworthy the definition of DA signal at this concentration level, considering the mild sample treatment, without overlapping of the UA wave at ca. + 360 mV, thus leading to successful DA quantification. Therefore, the diluted spiked urine samples were supplemented with two DA additions (2.0 μM each) and the neurotransmitter concentration was evaluated using the standard addition method. The results of these experiments yielded a mean concentration value of 42 μM ($n = 3$) in urine, with a standard deviation of 4.6 μM (RSD 10.9 %), resulting in a mean recovery of 104 %. The chromatographic analysis of whole urine samples confirmed the absence of DA whereas the recovery of DA in spiked samples was estimated to be 101 % (mean concentration 40.4 μM ; RSD 3.5 %; $n = 3$).

Table S7 within Supplementary Data presents analytical data regarding to the determination of DA and UA in human urine samples with other electroanalytical approaches. The results obtained with the proposed GA-rGO/GCE suggest an analytical performance comparable to that demonstrated by these representative examples, characterized by

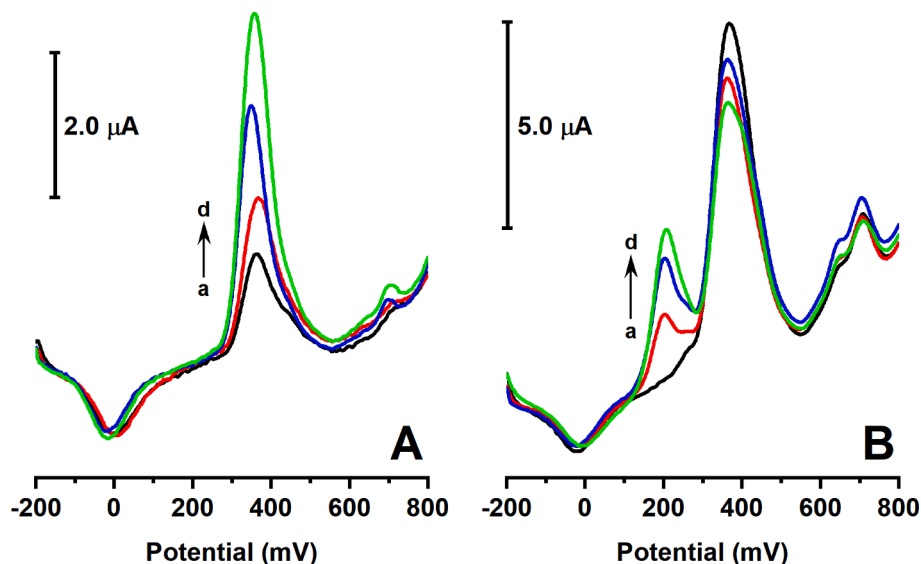


Fig. 6. (A) Stripping voltammograms of 200-fold diluted human urine sample (—) and successive additions of 20 μM UA and (B) 20-fold diluted blank (—; a) and DA spiked (—; b) human urine sample and successive additions of 2.0 μM DA to spiked sample (—; c, and —; d). Working electrode: GA-rGO/GCE. Supporting electrolyte: 0.050 M phosphate buffer solution of pH 7.0. Scan rate: 0.050 V s^{-1} . Accumulation time: 5.0 min.

using pulsed voltammetric techniques and involving electrode modifiers of intricate synthesis.

Conclusions

A simple one-step method has been successfully developed to produce reduced graphene oxide nanomaterials functionalized with phenolic groups (GA-rGO) using gallic acid and GO as precursors. Gallic acid, a natural phenolic compound, served as both a greener reducing agent and a stabilizing/functionalization element. Therefore, it played a key role in enhancing the dispersion ability and electrochemical properties of the resulting material. Spectroscopic techniques and electron microscopy were employed to characterize GA-rGO and its aqueous dispersions, confirming the efficient reduction of GO and the presence of phenolic related functional groups in these nanomaterials. GA-rGO was reproducibly incorporated onto the surface of a GCE through drop-coating of aqueous dispersions and the modified electrodes were characterized by cyclic voltammetry. The structural characteristics of the GA-rGO demonstrated a distinctive electroanalytical performance towards HZ, DA, AA, or UA, exhibiting lower overpotentials and higher sensitivity compared to bare GCE, and GCE modified with GO, HZ-rGO, and ERGO. Following the optimization of modification and measurement process, the proposed GA-rGO/GCE proved suitable for the selective determination of DA even in the presence of excess of AA and UA, in a simple way without need of permselective membranes or complex modification steps. This outstanding performance facilitated the reliable analysis of real samples, including medication products and human urine samples, where DA and UA were successfully quantified by AdSV.

This work unveils the promising electroanalytical application of nanomaterials derived from the reduction of graphene oxide using natural reducing agents, a topic scarcely reported to date. Appropriate functionalization can be achieved in a simple and more sustainable manner. The performance demonstrated herein by this GA-rGO open the doors to further applications of this type of nanomaterials in environmental and clinical fields. Electroanalysis based on GA-rGO/GCE might play a pivotal role in these areas, as well as in other fields such as biomaterials, composites, and energy-related technologies.

Declaration of Generative AI and AI-assisted technologies in the writing process.

During the preparation of the revised version of this work, the authors used ChatGPT 3.5 in order to enhance the language and ensure the grammatical correctness. After employing this tool/service, the authors reviewed and edited the content as necessary, taking full responsibility for the content of the publication.

CRedit authorship contribution statement

Mónica Moreno: Conceptualization, Methodology, Formal analysis, Supervision, Resources, Visualization, Writing – original draft, Writing – review & editing. **Alberto Sánchez Arribas:** Conceptualization, Methodology, Formal analysis, Supervision, Funding acquisition, Project administration, Resources, Writing – original draft, Writing – review & editing. **Silvia Royano:** Investigation, Formal analysis, Data curation, Visualization, Methodology. **Yaiza Izquierdo:** Investigation, Visualization. **Manuel Chicharro:** Conceptualization, Project administration, Resources.

Declaration of competing interest

The authors declare that they have no known competing financial interests or personal relationships that could have appeared to influence the work reported in this paper.

Data availability

Data will be made available on request.

Acknowledgments

The authors are grateful to the Spanish Ministry of Economy and Competitiveness (MINECO) and European Regional Development Fund (FEDER) for the financial support of the project (CTQ2015-64505-R). Community of Madrid and European Social Fund are acknowledged for supporting S. R. (PEJD-2019-PRE/IND-16584) and Y. I. (PEJ-2018-TL/IND-11539) contracts through the Youth Employment Initiative (YEI). The authors wish to thank Dra. Margarita Darder for her assistance in Raman Spectrometry analysis and Dra. M^a Angeles Martín for the access to freeze-drying facility.

Appendix A. Supplementary data

Supplementary data to this article can be found online at <https://doi.org/10.1016/j.flatc.2023.100605>.

References

- [1] Y. Wang, Z. Li, J. Wang, J. Li, Y. Lin, Graphene and graphene oxide: biofunctionalization and applications in biotechnology, *Trends in Biotechnol.* 29 (2011) 205–212, <https://doi.org/10.1016/j.tibtech.2011.01.008>.
- [2] S. Cinti, F. Arduini, Graphene-based screen-printed electrochemical (bio)sensors and their applications: efforts and criticisms, *Biosensors Bioelectron.* 89 (2017) 107–122, <https://doi.org/10.1016/j.bios.2016.07.005>.
- [3] H. Jin, C. Guo, X. Liu, J. Liu, A. Vasileff, Y. Jiao, Y. Zheng, S.Z. Qiao, Emerging two-dimensional nanomaterials for electrocatalysis, *Chem. Rev.* 118 (2018) 6337–6408, <https://doi.org/10.1021/acs.chemrev.7b00689>.
- [4] H. Shamkhalichenar, J.-W. Choi, Review—non-enzymatic hydrogen peroxide electrochemical sensors based on reduced graphene oxide, *J. Electrochem. Soc.* 167 (2020) 037531, <https://doi.org/10.1149/1945-7111/ab644a>.
- [5] A. Geim, K. Novoselov, The rise of graphene, *Nat. Mater.* 6 (2007) 183–191, <https://doi.org/10.1038/nmat1849>.
- [6] A. Obraztsov, Making graphene on a large scale, *Nature Nanotech.* 4 (2009) 212–213, <https://doi.org/10.1038/nnano.2009.67>.
- [7] F. Xi, D. Zhao, X. Wang, P. Chen, Non-enzymatic detection of hydrogen peroxide using a functionalized three-dimensional graphene electrode, *Electrochem. Commun.* 26 (2013) 81–84, <https://doi.org/10.1016/j.elecom.2012.10.017>.
- [8] K. Emtsev, A. Bostwick, K. Horn, K., et al., Towards wafer-size graphene layers by atmospheric pressure graphitization of silicon carbide, *Nat. Mater.* 8 (2009) 203–207, <https://doi.org/10.1038/nmat2382>.
- [9] D.R. Dreyer, S. Park, C.W. Bielawski, R.S. Ruoff, The chemistry of graphene oxide, *Chem. Soc. Rev.* 39 (2010) 228–240, <https://doi.org/10.1039/B917103G>.
- [10] R. Tarcán, O. Todor-Boer, I. Petrovai, C. Leordean, S. Astilean, I. Botiz, Reduced graphene oxide today, *J. Mater. Chem. C* 8 (2020) 1198–1224, <https://doi.org/10.1039/C9TC04916A>.
- [11] M.T.H. Aunkor, I.M. Mahbubul, R. Saidurb, H.S.C. Metselaar, The green reduction of graphene oxide, *RSC Adv.* 6 (2016) 27807–27828, <https://doi.org/10.1039/C6RA03189G>.
- [12] X. Wang, L. Zhi, K. Mullen, Transparent, conductive graphene electrodes for dye-sensitized solar cells, *Nano Lett.* 8 (2008) 323–327, <https://doi.org/10.1021/nl072838r>.
- [13] X. Xie, Y. Zhou, K. Huang, Advances in microwave-assisted production of reduced graphene oxide, article 355, *Front. Chem.* 7 (2019), <https://doi.org/10.3389/fchem.2019.00355>.
- [14] S.-H. Park, H.S. Kim, Environmentally benign and facile reduction of graphene oxide by flash light irradiation, *Nanotechnology* 26 (2015) 205601, <https://doi.org/10.1088/0957-4484/26/20/205601>.
- [15] S.J. Rowley-Neale, E.P. Randviir, A.S. Abo Dena, C.E. Banks, An overview of recent applications of reduced graphene oxide as a basis of electroanalytical sensing platforms, *Appl. Mater. Today* 10 (2018) 218–226, <https://doi.org/10.1016/j.apmt.2017.11.010>.
- [16] A. Ambrosi, C.K. Chua, N.M. Latiff, A.H. Loo, C.H.A. Wong, A.Y.S. Eng, A. Bonanni, M. Pumera, Graphene and its electrochemistry – an update, *Chem. Soc. Rev.* 45 (2016) 2458–2493, <https://doi.org/10.1039/C6CS00136J>.
- [17] J. Xu, Y. Wang, S. Hu, Nanocomposites of graphene and graphene oxides: Synthesis, molecular functionalization and application in electrochemical sensors and biosensors. A Review, *Microchim. Acta* 184 (2017) 1–44, <https://doi.org/10.1007/s00604-016-2007-0>.
- [18] D.A.C. Brownson, A.-G.-M. Ferrari, S. Ghosh, M. Kamruddin, J. Iniesta, C.E. Banks, Electrochemical properties of vertically aligned graphenes: tailoring heterogeneous electron transfer through manipulation of the carbon microstructure, *Nanoscale Adv.* 2 (2020) 5319–5328, <https://doi.org/10.1039/D0NA00587H>.
- [19] B. Wu, L. Xiao, M. Zhang, C. Yang, Q. Li, G. Li, Q. He, J. Liu, Facile synthesis of dendritic-like CeO₂/rGO composite and application for detection of uric acid and

- tryptophan simultaneously, *J. Solid State Chem.* 296 (2021) 122023, <https://doi.org/10.1016/j.jssc.2021.122023>.
- [20] S. Zhang, P. Ling, Y. Chen, J. Liu, C. Yang, 2D/2D porous Co₃O₄/rGO nanosheets act as an electrochemical sensor for voltammetric tryptophan detection, *Diam. Relat. Mater.* 135 (2023) 109811, <https://doi.org/10.1016/j.diamond.2023.109811>.
- [21] A. Karmakar, T. Mallick, S. Das, N.A. Begum, Naturally occurring green multifunctional agents: exploration of their roles in the world of graphene and related systems, *Nano-Structures & Nano-Objects* 13 (2018) 1–20, <https://doi.org/10.1016/j.nanoso.2017.10.005>.
- [22] A. Karmakar, T. Mallick, A. Pramanik, D. Mandal, N.A. Begum, Towards the development of antioxidant-wrapped graphene-based fluorescent nanomaterials having theragnostic potentials: a combined experimental and theoretical study, *Carbon Trends* 4 (2021) 100042, <https://doi.org/10.1016/j.cartre.2021.100042>.
- [23] A. Esfandiari, O. Akhavan, A. Irajizadeh, Melatonin as a powerful bio-antioxidant for reduction of graphene oxide, *J. Mater. Chem.* 21 (2011) 10907, <https://doi.org/10.1039/C1JM10151J>.
- [24] C. Silva, F. Simon, P. Friedel, P. Pötschke, C. Zimmerer, Elucidating the chemistry behind the reduction of graphene oxide using a green approach with polydopamine, *Nanomaterials* 9 (2019) 902, <https://doi.org/10.3390/nano9060902>.
- [25] A.A. Javidparvaz, R. Naderia, B. Ramezanzadeh, L-cysteine reduced/functionalized graphene oxide application as a smart/ control release nanocarrier of sustainable cerium ions for epoxy coating anticorrosion properties improvement, *J. Hazard. Mater.* 389 (2020) 122135, <https://doi.org/10.1016/j.jhazmat.2020.122135>.
- [26] D. Zhang, X. Zhang, Y. Chen, C. Wang, Y. Ma, An environment-friendly route to synthesize reduced graphene oxide as a supercapacitor electrode material, *Electrochim. Acta* 69 (2012) 364–370, <https://doi.org/10.1016/j.electacta.2012.03.024>.
- [27] Y. Feng, N. Feng, G. Du, A green reduction of graphene oxide via starch-based materials, *RSC Adv.* 3 (2013) 21466–21474, <https://doi.org/10.1039/C3RA43025A>.
- [28] K.B. Narayanan, G.T. Park, S.S. Han, Antibacterial properties of starch-reduced graphene oxide–polyiodide nanocomposite, *Food Chem.* 342 (2021) 128385, <https://doi.org/10.1016/j.foodchem.2020.128385>.
- [29] J. Luo, N. Zhang, J.P. Lai, R. Liu, X.Y. Liu, Tannic acid functionalized graphene hydrogel for entrapping gold nanoparticles with high catalytic performance toward dye reduction, *J. Hazard. Mater.* 300 (2015) 615–623, <https://doi.org/10.1016/j.jhazmat.2015.07.079>.
- [30] Y. Li, S. Shi, H. Cao, R. Cao, Robust antifouling anion exchange membranes modified by graphene oxide (GO)-enhanced co-deposition of tannic acid and polyethylenimine, *J. Membr. Sci.* 625 (2021) 119111, <https://doi.org/10.1016/j.memsci.2021.119111>.
- [31] J. Li, G. Xiao, C. Chen, R. Li, D. Yan, Superior dispersions of reduced graphene oxide synthesized by using gallic acid as a reductant and stabilizer, *J. Mater. Chem. A* 1 (2013) 1481–1487, <https://doi.org/10.1039/C2TA00638C>.
- [32] Z. Wang, L. Jiang, H. Pan, Y. Cui, C. Zong, Green and facile preparation of graphene/resveratrol/polyaniline composites for high-performance supercapacitors, *New J. Chem.* 45 (2021) 3581–3588, <https://doi.org/10.1039/d0nj04739b>.
- [33] S. Gurunathan, J.W. Han, E.S. Kim, J.H. Park, J.H. Kim, Reduction of graphene oxide by resveratrol: a novel and simple biological method for the synthesis of an effective anticancer nanotherapeutic molecule, *Int. J. Nanomedicine* 10 (2015) 2951–2969, <https://doi.org/10.2147/IJN.S79879>.
- [34] F. Bugli, M. Cacaci, V. Palmieri, R. Di Santo, R. Torelli, G. Ciasca, M. Di Vito, A. Vitali, C. Conti, M. Sanguinetti, M. De Spirito, M. Papi, Curcumin-loaded graphene oxide flakes as an effective antibacterial system against methicillin-resistant *Staphylococcus aureus*, *Interface Focus* 8 (2018) 20170059, <https://doi.org/10.1098/rsfs.2017.0059>.
- [35] S. Hatamie, O. Akhavan, S.K. Sadrnezhad, M.M. Ahadian, M.M. Shirokhar, H. Q. Wang, Curcumin-reduced graphene oxide sheets and their effects on human breast cancer cells, *Mater. Sci. Eng. C* 55 (2015) 482–489, <https://doi.org/10.1016/j.msec.2015.05.077>.
- [36] Z. Ismail, Green reduction of graphene oxide by plant extracts: a short review, *Ceram. Int.* 45 (2019) 23857–23868, <https://doi.org/10.1016/j.ceramint.2019.08.114>.
- [37] Y. Yang, W. Ma, Z. Li, Z. Zhang, Z. Hu, Graphene non-covalently functionalized with Gallic acid (Ga) as high performance electrode material for supercapacitors, *J. Sci.: Adv. Mater. Devices* 7 (2022) 100386, <https://doi.org/10.1016/j.jsamd.2021.07.009>.
- [38] Z. Gan, T. Wang, C. Zhai, J. Ma, R. Cao, Y. Wang, Gallic acid-reduced graphene oxide deposited with carbon nanotubes for transparent film heaters, *ACS Appl. Electron. Mater.* 5 (2023) 1148–1155, <https://doi.org/10.1021/acsaem.2c01617>.
- [39] D. Li, M.B. Müller, R.B. Scott Gilje, G.G. Kaner, Wallace, Processable aqueous dispersions of graphene nanosheets, *Nat. Nanotechnol.* 3 (2008) 101–105, <https://doi.org/10.1038/nnano.2007.451>.
- [40] S. Parrot, P.-C. Nauzeret, L. Denoroy, A rapid and sensitive method for the analysis of brain monoamine neurotransmitters using ultra-fast liquid chromatography coupled to electrochemical detection, *J. Chromatogr. B* 879 (2011) 3871–3878, <https://doi.org/10.1016/j.jchromb.2011.10.038>.
- [41] R. Liao, Z. Tang, Y. Lei, B. Guo, Polyphenol-reduced graphene oxide: mechanism and derivatization, *J. Phys. Chem. C* 115 (2011) 20740–20746, <https://doi.org/10.1021/jp2068683>.
- [42] V. Tucureanu, A. Matei, A.M. Avram, FTIR spectroscopy for carbon family study, *Crit. Rev. Anal. Chem.* 46 (2016) 502–520, <https://doi.org/10.1080/10408347.2016.1157013>.
- [43] R. M. Silverstein; F. X. Webster; D. J. Kiemle; Spectrometric identification of organic compounds. Seventh edition. John Wiley & Sons. Inc. New York. 2005. ISBN 0-471-39362-2; pp. 89-90.
- [44] I.Y. Tóth, M. Szekeres, R. Turcu, S. Sáringer, E. Illés, D. Nesztör, E. Tombácz, Mechanism of in situ surface polymerization of gallic acid in an environmental-inspired preparation of carboxylated core-shell magnetite nanoparticles, *Langmuir* 30 (2014) 15451–15461, <https://doi.org/10.1021/la5038102>.
- [45] J. López, J.M. Hernández-Alcántara, P. Roquero, C. Montiel, K. Shirai, M. Gimeno, E. Bárzana, Trametes versicolor laccase oxidation of gallic acid toward a polyconjugated semiconducting material, *J. Mol. Catal. B: Enzym.* 97 (2013) 100–105, <https://doi.org/10.1016/j.molcatb.2013.07.020>.
- [46] J.H. Lehman, M. Terrones, E. Mansfield, K.E. Hurst, V. Meunier, Evaluating the characteristics of multiwall carbon nanotubes, *Carbon* 49 (2011) 2581–2602, <https://doi.org/10.1016/j.carbon.2011.03.028>.
- [47] R. Beams, L.G. Cançado, L. Novotny, Raman characterization of defects and dopants in graphene, *J. Phys.: Condens. Matter* 27 (2015) 083002, <https://doi.org/10.1088/0953-8984/27/8/083002>.
- [48] S.L.H. Rebelo, A. Guedes, M.E. Szeftczyk, A.M. Pereira, J.P. Araújo, C. Freire, Progress in the Raman spectra analysis of covalently functionalized multiwalled carbon nanotubes: unraveling disorder in graphitic materials, *Phys. Chem. Chem. Phys.* 18 (2016) 12784–12796, <https://doi.org/10.1039/C5CP06519D>.
- [49] J.-B. Wu, M.-L. Lin, X. Cong, H.-N. Liu, P.-H. Tan, Raman spectroscopy of graphene-based materials and its applications in related devices, *Chem. Soc. Rev.* 47 (2018) 1822–1873, <https://doi.org/10.1039/C6CS00915H>.
- [50] S. Claramunt, A. Varea, D. López-Díaz, M.M. Velázquez, A. Cornet, A. Cirera, The Importance of Interbands on the Interpretation of the Raman Spectrum of Graphene Oxide, *J. Phys. Chem. C* 119 (2015) 10123–10129, <https://doi.org/10.1021/acs.jpcc.5b01590>.
- [51] A.C. Ferrari, Raman spectroscopy of graphene and graphite: Disorder, electron-phonon coupling, doping and nonadiabatic effects, *Solid State Commun.* 143 (2007) 47–57, <https://doi.org/10.1016/j.ssc.2007.03.052>.
- [52] X. Díez-Betruí, S. Álvarez-García, C. Botas, P. Álvarez, J. Sánchez-Marcos, C. Prieto, R. Menéndez, A. de Andrés, Raman spectroscopy for the study of reduction mechanisms and optimization of conductivity in graphene oxide thin films, *J. Mater. Chem. C* 1 (2013) 6905–6912, <https://doi.org/10.1039/C3TC31124D>.
- [53] E.H. Martins Ferreira, V.O. Marcus, F. Moutinho, M.M. Stavale, R.B. Lucchese, C. A. Capaz, Achete, A. Jorio, Evolution of the Raman spectra from single-, few-, and many-layer graphene with increasing disorder, *Phys. Rev. B* 82 (2010) 125429, <https://doi.org/10.1103/PhysRevB.82.125429>.
- [54] K. Zhang, J. Wang, J. Zou, W. Cai, Q. Zhang, Low excitation of Raman D-band in [2 +1] cycloaddition functionalized single-walled carbon nanotubes, *Carbon* 138 (2018) 188–196, <https://doi.org/10.1016/j.carbon.2018.05.073>.
- [55] H.R. Zare, A.M. Habibirad, Electrochemistry and electrocatalytic activity of catechin film on a glassy carbon electrode toward the oxidation of hydrazine, *J. Solid State Electrochem.* 10 (2006) 348–359, <https://doi.org/10.1007/s10008-005-0683-5>.
- [56] C. Wang, L. Zhang, Z. Guo, J. Xu, H. Wang, K. Zhai, X. Zhuo, A novel hydrazine electrochemical sensor based on the high specific surface area graphene, *Microchim. Acta* 169 (2010) 1–6, <https://doi.org/10.1007/s00604-010-0304-6>.
- [57] I. Ferrari, A. Motta, R. Zanoni, F.A. Scaramuzza, F. Amato, E.A. Dalchiale, A. G. Marrani, Understanding the nature of graphene oxide functional groups by modulation of the electrochemical reduction: a combined experimental and theoretical approach, *Carbon* 203 (2023) 29–38, <https://doi.org/10.1016/j.carbon.2022.11.052>.
- [58] M. Gao, Y. Xu, X. Wang, Y. Sang, S. Wang, Analysis of electrochemical reduction process of graphene oxide and its electrochemical behavior, *Electroanalysis* 28 (2016) 1377–1382, <https://doi.org/10.1002/elan.201501063>.
- [59] M. Bagherzadeh, M. Heydari, Electrochemical detection of dopamine based on pre-concentration by graphene nanosheets, *Analyst* 138 (2013) 6044–6051, <https://doi.org/10.1039/c3an01318a>.
- [60] R.L. McCreery, Advanced carbon electrode materials for molecular electrochemistry, *Chem. Rev.* 108 (2008) 2646–2687, <https://doi.org/10.1021/cr068076m>.
- [61] M.M. Rahman, J.-J. Lee, Electrochemical dopamine sensors based on graphene, *J. Electrochem. Sci. Technol.* 10 (2019) 185–195, <https://doi.org/10.5229/JECST.2019.10.2.185>.
- [62] I. Lavagnini, R. Antiochia, F. Magno, An extended method for the practical evaluation of the standard rate constant from cyclic voltammetric data, *Electroanalysis* 16 (2004) 505–506, <https://doi.org/10.1002/elan.200302851>.
- [63] M.M. Rahman, D. Liu, N.S. Lopa, J.-B. Baek, C.-H. Nam, J.-J. Lee, Effect of the carboxyl functional group at the edges of graphene on the signal sensitivity of dopamine detection, *J. Electroanal. Chem.* 898 (2021) 115628, <https://doi.org/10.1016/j.jelechem.2021.115628>.